Article

Histones Cause Aggregation and Fusion of Lipid Vesicles Containing Phosphatidylinositol-4-Phosphate

Marta G. Lete,[1,2] Jesus Sot,[1,2] David Gil,[3] Mikel Valle,[3] Milagros Medina,[4,5] Felix M. Goñi,[1,2] and Alicia Alonso[1,2,*]
[1]Unidad de Biofísica (CSIC, UPV/EHU) and [2]Departamento de Bioquímica, Universidad del País Vasco, Leioa, Spain; [3]Structural Biology Unit, Center for Cooperative Research in Biosciences, CIC bioGUNE, Derio, Spain; and [4]Departamento de Bioquímica y Biología Molecular y Celular, Facultad de Ciencias and [5]Instituto de Biocomputación y Física de Sistemas Complejos, Unidad Asociada BIFI-IQFR, Universidad de Zaragoza, Zaragoza, Spain

ABSTRACT In a previous article, we demonstrated that histones (H1 or histone octamers) interact with negatively charged bilayers and induce extensive aggregation of vesicles containing phosphatidylinositol-4-phosphate (PIP) and, to a lesser extent, vesicles containing phosphatidylinositol (PI). Here, we found that vesicles containing PIP, but not those containing PI, can undergo fusion induced by histones. Fusion was demonstrated through the observation of intervesicular mixing of total lipids and inner monolayer lipids, and by ultrastructural and confocal microscopy studies. Moreover, in both PI- and PIP-containing vesicles, histones caused permeabilization and release of vesicular aqueous contents, but the leakage mechanism was different (all-or-none for PI and graded release for PIP vesicles). These results indicate that histones could play a role in the remodeling of the nuclear envelope that takes place during the mitotic cycle.

INTRODUCTION

Phosphoinositides and their derivatives are known to play an important role as second messengers in cell dynamics (1–3). They have also been shown to be important agents in modulating the morphology of the endoplasmic reticulum (ER) and its subcompartment, the nuclear envelope (NE) (4–6). The NE is disassembled and reassembled through fission and fusion events, respectively, during each cycle of mitosis. Byrne et al. (7) reported that phosphoinositides play an important role in regulating NE assembly during formation of the male pronucleus in an echinoderm model. They showed that a non-ER membrane fraction (MV1) enriched in phospholipase Cγ and Src kinase, and with very high levels of phosphoinositides, was critical for NE formation (7). It should be noted that the NE is no longer viewed as a smooth sheet covering chromatin, but rather as a dynamic structure that includes invaginations that penetrate deep into the nucleoplasm (8,9).

This complex and dynamic view of the NE and its component the nucleoplasmic reticulum elicits, almost by necessity, questions about the possible interactions of NE and chromatin. In particular, the presence of histones and other positively charged proteins in chromatin raises the possibility that these proteins interact with negatively charged lipids in the nuclear membrane. In fact, several authors (10–12) have studied the interaction of histones with phosphatidylserine and other negatively charged lipids that exist in very minor amounts in the NE. In a previous study (13), we found that a variety of histone and histone combinations (H1, H2AH2B, H3H4, and octamers) caused a dose-dependent aggregation of phospholipid vesicles composed mainly of phosphatidylcholine (PC) to which 5–20 mol % phosphoinositides was added. We observed that 5 mol % phosphatidylinositol-4-phosphate (PIP) was enough to cause extensive vesicle aggregation under our conditions, which we interpreted as a (mostly electrostatic) interaction between histones and PIP. With phosphatidylinositol (PI), at least 20 mol % was necessary to observe a similar degree of aggregation. Isothermal calorimetry data for the lipid-protein interaction were compatible with phosphoinositide/histone stoichiometries of ~0.5 (PIP) and ~1.0 (PI), respectively. Moreover, competition experiments involving histones and negatively charged vesicles and DNA demonstrated the possibility of coexisting DNA- and PIP-bound histones (13).

The current views of NE structure suggest a complex interplay of histones, DNA, and phosphoinositides, particularly in the deep recesses of the nucleoplasmic reticulum. Because of the extensive fission/fusion events that take place at the NE during the mitotic cycle (8,14), we were tempted to explore the putative role of histone-membrane interactions in such a series of events. Moreover, we had observed (13) aggregation of charged vesicles in the presence of histones, and vesicle-vesicle aggregation is a prerequisite for (though not a sufficient cause of) vesicle fusion (15–19). In this study, we show the capacity of histones to induce fusion in PIP-containing vesicles, in addition to aggregation, intervesicular lipid mixing, and intervesicular

Submitted November 3, 2014, and accepted for publication December 9, 2014.

*Correspondence: alicia.alonso@ehu.es

Editor: Francesca Marassi.

0006-3495/15/02/0863/9 $2.00

http://dx.doi.org/10.1016/j.bpj.2014.12.018

mixing of inner monolayer lipids. These data, together with ultrastructural evidence, demonstrate histone-induced vesicle-vesicle fusion.

MATERIALS AND METHODS

Materials

Egg PC was purchased from Lipid Products (South Nutfield, UK). PI, PIP, and lissamine rhodamine PE (Rho-PE) were supplied by Avanti Polar Lipids (Alabaster, AL). Histones were obtained from chicken (*Gallus gallus*) erythrocyte chromatin as previously described by Wang et al. (20). Alexa Fluor 488 histone H1 (H1-Alexa488), Rho B 1,2-dihexadecanoyl-*sn*-glycero-3-phosphoethanolamine, triethylammonium salt (Rho-DHPE), 8-aminoaphthalene-1,3,6-trisulfonic acid, disodium salt (ANTS), *p*-xylene-bis-pyridinium bromide (DPX), N-(7nitrobenz-2-oxa-1,3-diazol-4-yl)-3-phophoethanolamine triethylamine salt (NBD-PE), and 1,1′-dioctadecyl-3,3,3′,3′-tetramethylindodicarbocyanine, 4-chlorobenzenesulfonate salt (DiD) were obtained from Molecular Probes (Eugene, OR). Bis [N,N′bis(carboxymethyl)aminomethyl]fluorescein (calcein), resin Sephacryl 500-HR (Poly([allyl dextran]-co-N,N′-methylenebisacrylamide), and sodium dithionite were supplied by Sigma (St. Louis, MO). Disposable PD-10 desalting columns (Sephadex G-25 medium) were purchased from General Electric (Buckinghamshire, UK). For lifetime assays, a chromatography column of 1.0 × 30 cm (diameter × length) from BioRad was utilized. All other materials (salts and organic solvents) were of analytical grade.

Liposome preparation

The appropriate lipids were mixed in organic solution and the solvent was evaporated to dryness under a stream of N_2. Then the sample was kept under vacuum for 2 h to remove solvent traces. The lipids were swollen in 10 mM Hepes, 150 mM NaCl, pH 7.4 buffer. Large unilamellar vesicles (LUVs) were prepared from the swollen lipids, subjected to 10 freeze/thaw cycles, and then extruded using 0.1 μm pore size Nuclepore filters as described by Mayer et al. (21). We checked the vesicle size by quasi-elastic light scattering using a Malvern Zeta-Sizer 4 spectrometer (Malvern Instruments, Worcestershire, UK). The LUVs had an average diameter of ~100 nm. Calcein-loaded LUVs (200 nm) were passed through disposable filters (Anatop 10; Whatman, Germany) via 1 ml plastic syringes. Lipid concentration was determined by phosphate analysis (22).

Lipid mixing assays

Lipid mixing was assayed by steady-state Forster resonance energy transfer (FRET) as previously described (23) using NBD-PE and Rho-DHPE. Vesicles containing 2% NBD-PE, 2% Rho-DHPE in their bilayer composition were mixed with probe-free liposomes at a 1:4 ratio. NBD-PE emission was followed at 530 nm (excitation wavelength at 465 nm) with a cutoff filter at 515 nm between the sample and the emission monochromator to avoid scattering interferences. Zero percent mixing was established as the equilibrium fluorescence emission in the absence of histone, and 100% mixing was set after addition of Triton X-100. All fluorescence assays were performed at room temperature under continuous stirring in an Aminco Bowman Series 2 luminescence spectrometer. Lipid and protein concentrations were 0.3 mM and 10 μg/ml, respectively.

Intervesicular lipid mixing alone does not prove vesicle fusion, because lipid mixing can also be observed in the phenomenon called hemifusion (24) or close apposition (25), in which the lipids of the outer monolayers of two adjoining vesicle membranes are mixed without the occurrence of fusion. To overcome this problem, one can apply a technique that allows direct observation of mixing of the inner monolayer lipids (26). Naturally, this occurs only when a fusion process takes place, and thus detection of intervesicular mixing of inner monolayer lipids is diagnostic for vesicle-vesicle fusion. The procedure is also based on FRET between two vesicle populations, but in this case the fluorescence probes in the outer monolayer are chemically bleached with the membrane-impermeable dithionite so that only variations in intensity arising from the inner monolayer are recorded.

For inner lipid mixing, the NBD in the outer monolayer was quenched by adding 1–2 μl of 100 mM dithionite solution stepwise to the labeled LUV until its initial fluorescence intensity was reduced to one-half. Immediately after they were quenched, the LUVs were passed through a Sephadex G-25 chromatography column to remove the dithionite from the LUV solution. The same buffer in which the liposomes were prepared was used as an eluent.

Stopped-flow kinetics

Since the initial stages of both lipid mixing and leakage (23) occur very rapidly, a rapid kinetics device is required to record these events. For this purpose, we performed stopped-flow studies using an Applied Photophysics SX17.MV instrument equipped with a fluorescence detector and Pro-Data SX software. Measurements were carried out in 10 mM Hepes, 150 mM NaCl, pH 7.4 at 25°C with the same volumes of reactants in the stopped-flow syringes, and the concentrations after mixing were 0.3 mM for LUVs and 10 μg/ml for H1, corresponding to approximately 1000/1 lipid:protein mole ratio.

We recorded the time courses by exciting each fluorophore at the appropriate wavelength (ANTS $\lambda_{exc} = 355$ nm, NBD $\lambda_{exc} = 465$ nm) and collecting the emission using adequate cutoff filters ($\lambda_{em} > 500$ nm).

The collected data for lipid mixing assays were fit to a single-exponential model ($y = A.e^{-kobs.t} + y_0$), which allowed us to determine the observed rate constant for the process (k_{obs}). In contrast, a two-exponential model ($y = A_1.e^{-kobs1.t} + A_2^{-kobs2.t} + y_0$) was required to fit the leakage-assay data because the dye can be either free in solution or partially entrapped. In these equations, y is the fluorescence intensity at time t, A (A_1, A_2, …) is the amplitude of each particular process, k_{obs} (k_{obs1}, k_{obs2}, …) is the observed rate constant for each observed process, and y_0 is the final fluorescence point. To calculate the initial rates of the different processes, these equations were differentiated and the slopes at $x = 0$ were measured.

Cryo-electron microscopy

Samples were placed in the controlled environment of a Vitrobot (FEI) vitrification chamber at room temperature, and the relative humidity was kept close to saturation to prevent water evaporation from the sample. A 5 μl drop of the aqueous solution was placed on carbon-coated holey film supported by a transmission electron microscopy (TEM) copper grid. Most of the liquid was removed by careful blotting with absorbent filter paper to create a thin liquid film. The sample was then rapidly plunged into liquid ethane and cooled by liquid nitrogen to its melting temperature to obtain a vitrified film. The vitrified specimen was stored under liquid nitrogen and then transferred to an electron microscope (Jeol JEM-2200FS) operating at 200 kV. Images were collected under low-dose conditions on a CCD camera (UltraScan 4000; Gatan) with an underfocus in the range of 3–5 μm at magnifications of 40,000–60,000×.

Preparation and observation of giant unilamellar vesicles

Giant unilamellar vesicles (GUVs) were prepared using the electroformation method developed by Angelova and Tsoneva (27). GUVs were formed in a PRETGUV 4 chamber supplied by Industrias Técnicas ITC (Bilbao, Spain). Stock solutions of lipids (0.2 mM total lipid containing either 0.2 mol % Rho-PE or 0.4 mol % DiD) were prepared in

chloroform/methanol (2:1, v/v). Then, 3 μl of the lipid stocks were added to the surface of Pt electrodes and solvent traces were removed by evacuating the chamber under high vacuum for at least 2 h.

The Pt electrodes were covered with 500 μL of a 300 mM sucrose solution that was previously heated at 37°C. The Pt electrodes were connected to a generator (TG330 function generator; Thurlby Thandar Instruments) under AC field conditions (10 Hz, 1 V_{RMS} for 2 h, followed by 1 Hz, 1 V_{RMS}, for 10 min) at 37°C. Finally, the AC field was turned off and the vesicles (in 300 mM sucrose) were collected from the PRETGUV 4 chamber with a pipette.

Separately, LUVs were prepared as described above with different dyes (2% DiD or 2% NBD-PE) in a buffer solution (10 mM Hepes, pH 7.4, 150 mM NaCl) of equal osmolarity to the GUV solution.

First, H1-Alexa488 was added to GUVs and gently mixed with the pipette. After a 30 min incubation, LUVs were added to the mix and everything was transferred to chambers pretreated with bovine serum albumin (2 mg/ml) and containing an isoosmotic buffer solution of 10 mM Hepes, pH 7.4, 150 mM NaCl. Due to the different densities of the two solutions, the vesicles sedimented at the bottom of the chamber, thus facilitating observation under the microscope.

The excitation wavelengths were 488 nm for H1-Alexa488 and NBD-PE, 561 nm for Rho-PE, and 637 nm for DiD. Images were collected using band-pass filters of 515 ± 15 nm for Alexa488 and NBD-PE, 593 ± 20 nm for Rho-PE, and a long-pass filter of 650 nm for DiD. All of these experiments were performed at room temperature. Image treatment was performed using EZ-C1 3.20 (Nikon) software.

Leakage assays

For leakage assays, ANTS and DPX were coencapsulated in a single liposome population so that DPX would quench most of the ANTS fluorescence (10 mM Hepes, pH 7.4, 40 mM NaCl, 12.5 mM ANTS, 45 mM DPX) (28). A Sephadex G-25 chromatography column was used to separate liposomes from nonencapsulated probes, with an equi-osmolar buffer (10 mM Hepes, pH 7.4, 150 mM NaCl) used as the eluent. Osmolality was checked using an Osmomat 030 cryoscopic osmometer (Gonotec, Berlin, Germany). Solutions were corrected for perfect isotonicity inside and outside the vesicles by adding small volumes of concentrated NaCl up to 0.310 (Osm/kg). The LUVs were diluted as required (usually to 0.3 mM) with assay buffer in a spectroscopy cuvette, and fluorescence was recorded continuously (excitation, 355 nm; emission, 520 nm; 450 nm cutoff filter). The basal signal obtained under these conditions was considered as 0% leakage. Then, 10 μg/ml of histones was added and increases in fluorescence were recorded. A 100% leakage signal was obtained by adding Triton X-100 to liposomes for lysis after equilibrium was reached. All leakage assays were performed at room temperature under continuous stirring in an Aminco Bowman Series 2 luminescence spectrometer.

Lifetime measurements

To determine the leakage mechanism, the calcein lifetime was measured as follows (29): first, calcein-loaded vesicles were prepared (10 mM Hepes, pH 7.4, 70 mM calcein, 0.5 mM EDTA). A 30 cm chromatography column was then packed with Sephacryl 500-HR and used to separate liposomes from nonencapsulated probe with an isoosmotic buffer (10 mM Hepes, pH 7.4, 100 mM NaCl, 0.5 mM EDTA). Aliquots of these vesicles were incubated for 1 h with increasing histone concentrations at 25°C in a thermomixer. The sample fluorescence was measured in a Fluoromax-3 spectrophotometer (Jobin Ybon; Horiba, Edison, NJ).

The curve for calcein-loaded vesicles in the absence of permeabilizer follows a biexponential behavior with a dominant B_E (E for entrapped) with a $\tau_e = 0.4$ ns, and a weak B_{F0} (F for free) with $\tau_e = 4.0$ ns from some remaining nonentrapped dye. When only some vesicles are leaky and release all entrapped dye while others remain intact, we speak of an all-or-none leakage mechanism, and calcein lifetimes remain the same as for calcein-loaded vesicles without the permeabilizer. On the other hand, if all of the vesicles release a certain amount of their contents, which we refer to as the graded mechanism, the lifetime of entrapped calcein (B_E) increases with increasing permeabilizer concentration because of the vesicles that are partially unloaded.

RESULTS

Lipid mixing

In view of the capacity of histones to induce aggregation of negatively charged vesicles, we assessed the possibility of histone-induced intervesicular lipid mixing. By adding histones and monitoring NBD-PE changes in fluorescence, we observed intervesicle lipid mixing in PC/PIP (9:1) vesicles. In the case of PI-containing liposomes, we did not observe any fluorescence changes or lipid mixing.

The results in Fig. 1 show that histones induce both total and inner monolayer lipid mixing, with the former denoting a special form of vesicle-vesicle intimate apposition, and the latter serving as a diagnostic for the opening of intervesicle pores (i.e., of membrane fusion). Histone (Fig. 1 *A*) produces lipid mixing, as shown by the increased NBD-PE fluorescence due to the dilution of probes in the membrane plane, which hinders the occurrence of FRET. Histone H1, H2AH2B, H3H4, and octamer give rise to different extents and rates of lipid mixing (Fig. 1, *C* and *D*). Inner monolayer mixing was demonstrated by the experiments shown in Fig. 1, *B–D*. Total and inner monolayer extents and rates varied in parallel, with the former being a prerequisite for the latter to occur (16). As in the leakage assays, the H1 initial rate is so much higher than the one produced by the core histones that it cannot be reliably measured. Note that the scales (*Y* axis) for total and inner monolayer lipid mixing are not the same: 100% mixing in the latter case refers to 100% of the lipid molecules in the inner monolayer, i.e., about one-half of the total lipid molecules.

Consequently, stopped-flow assays were performed to visualize the first stages of H1-induced lipid mixing. Lipid mixing was not observed when vesicles contained 10% of PI (Fig. 2 *A*), but both total and inner lipid mixing occurred in PIP-containing vesicles (Fig. 2 *B*). Time courses were fit to monoexponentials with observed rates of 1.2 ± 0.3 s^{-1} (R^2 0.94 ± 0.01) for total lipid mixing and 0.65 ± 0.15 s^{-1} (R^2 0.95 ± 0.02) for inner lipid mixing. Due to the different experimental conditions, the parameters measured in conventional and stopped-flow time-course experiments cannot be directly compared. In the former case, a relative 0–100% scale of lipid mixing is built and the rate units are specifically in % units × s^{-1}. This explains why the observed rate of H1-induced total lipid mixing, as measured by stopped-flow assays, is about twice that of the inner monolayer mixing, since in the former case the number of lipid molecules undergoing intervesicular exchange is twice as high as in the latter condition.

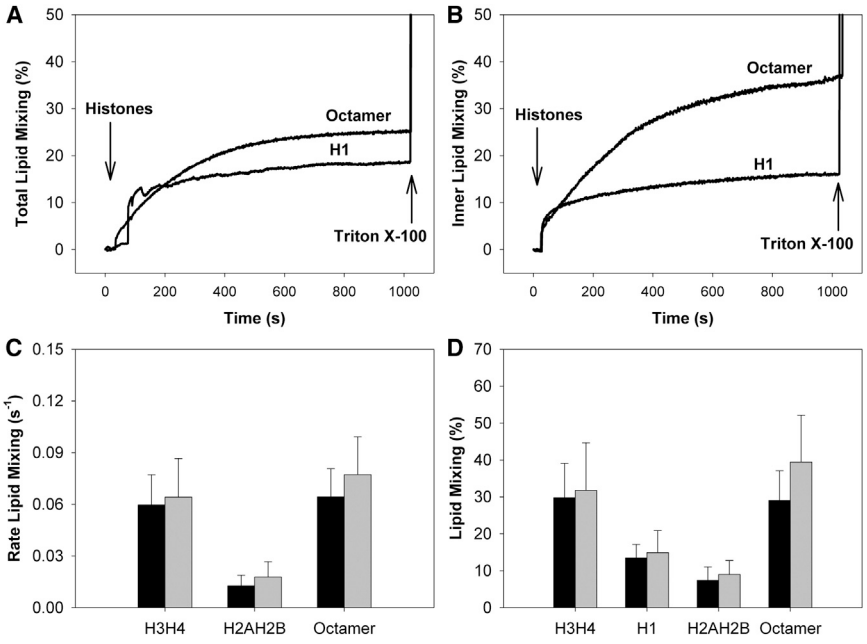

FIGURE 1 Histone-induced intervesicular lipid mixing. Assays with PC/PIP (9:1) LUVs. (*A*) Total lipid mixing time course. (*B*) Inner monolayer lipid mixing time course. Arrows indicate the histone or detergent addition. (*C*) Initial rates of lipid mixing produced by the different histone preparations. (*D*) Extent of lipid mixing produced by different histones under apparent equilibrium (~20 min). Black bars correspond to total lipid mixing and gray bars correspond to inner monolayer lipid mixing. Average values + mean ± SE ($n = 3$).

Cryo-TEM images

Cryo-TEM images were acquired before and after H1 addition to PC LUVs with 10 mol % of either PI or PIP (Fig. 3). With PI, the LUVs retained their morphology after H1 addition (*top-left panel*), whereas when PIP was present, a vast aggregation of LUVs was observed together with multiple events of vesicle-vesicle fusion (*bottom-left panel*). In this PIP+H1 sample, even regions with low concentration show a clear clustering of LUVs where the vesicle-vesicle

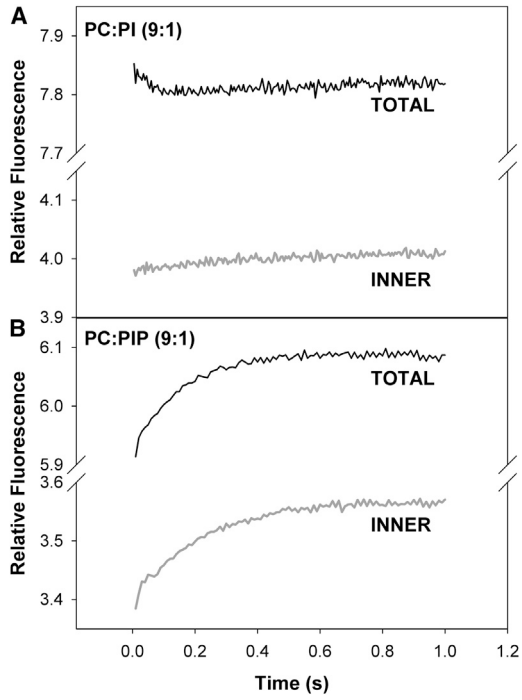

FIGURE 2 Early stages of H1-induced lipid mixing. Stopped-flow assay. Black, total lipid mixing; gray, inner lipid mixing. (*A*) LUV composed of PC/PI (9:1). (*B*) LUV composed of PC/PIP (9:1).

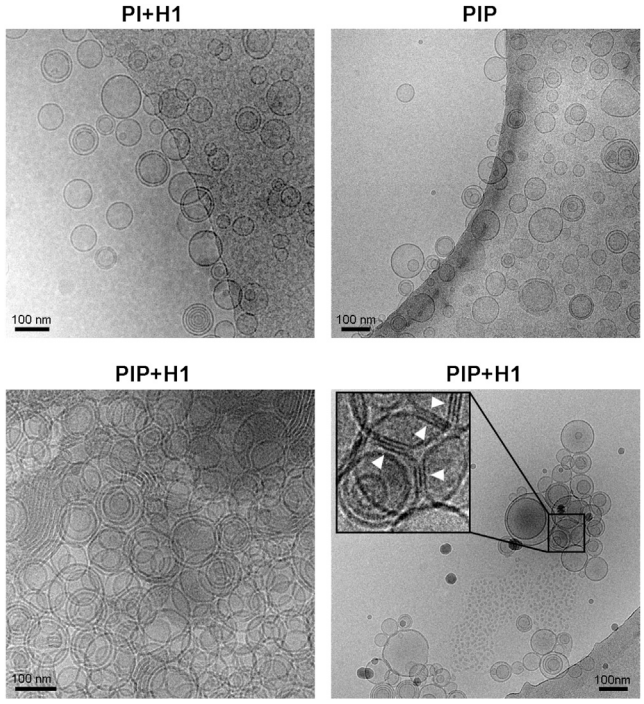

FIGURE 3 Cryo-TEM images of phosphoinositides containing LUVs with and without H1. Top right: control PC/PIP (9:1) vesicles. Top left: PC/PI (9:1) vesicles treated with H1 histone. Bottom: two views of PC/PIP vesicles treated with H1 histone. Inset in bottom-right picture: detail at a higher magnification. Scale bars: 100 nm.

intimate apposition is clearly observed in the images (*arrowheads, inset in bottom-right panel*). A gallery of cryo-TEM images of PI- and PIP-vesicles in the presence of histones can be found in the Supporting Material.

Confocal microscopy

Confocal microscopy enabled us to visualize lipid mixing between vesicles. PC/PIP (9:1) GUVs and LUVs containing different fluorescent probes (RhoPE in GUVs, and DiD in LUVs) were formed. GUVs and LUVs were mixed, treated with H1, and visualized under the confocal fluorescence microscope.

GUVs were observed in red with a blue background (Fig. 4 *A*), with the latter corresponding to LUVs that could not be seen individually due to the microscope's technical limitations. Note that in the bottom-left image of Fig. 4 *A*, no H1 is present (control experiment). When H1-Alexa488 was added (Fig. 4 *B*), we observed that both types of vesicles now contained the two lipid dyes, indicating that lipid mixing had occurred. Extensive aggregation of vesicles was also observed: LUVs appeared in patches and not as a homogeneous background. The vesicles were also profusely decorated with Alexa-stained histone molecules, indicating that the protein was the binding element between vesicles.

To visualize fusogenic processes, we monitored lipid mixing of the inner monolayer. The fusion process was carried out with GUVs stained with DiD and LUVs labeled with NBD-PE. The LUVs' outer membrane fluorescence was quenched with dithionite, so their fluorescence in this assay was only due to the inner monolayer of the vesicle membrane. Subsequently, the vesicle mix was treated with H1 and visualized under the microscope (Fig. 5). Labeled H1 could not be used in this assay because the spectrum of Alexa488 overlapped with that of NBD. Extensive LUV aggregation gave rise to a red mass of coalescent vesicles. Lipid mixing was observed as well through the overlapping of both dyes at the GUV membrane level, thus confirming that fusogenic processes that involve the inner monolayer lipid mixing were taking place.

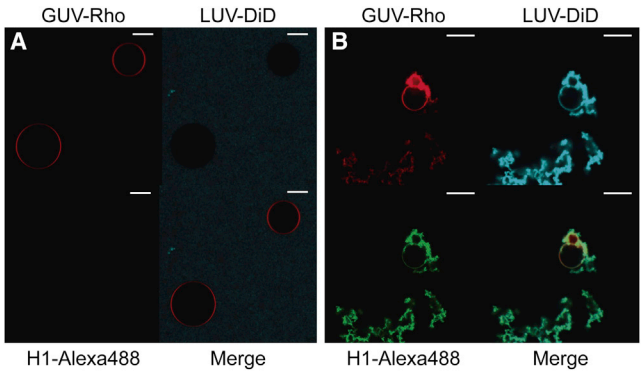

FIGURE 4 Total lipid mixing observed by confocal microscopy of representative PC/PIP (9:1) GUVs containing Rho (*red*) and LUVs containing DiD (*blue*) stains. (*A*) Control images obtained when H1-Alexa488 was not present. (*B*) GUVs and LUVs after H1-Alexa488 addition; vesicles now contain both dyes and H1 is also part of the aggregates. Scale bars: 10 μm.

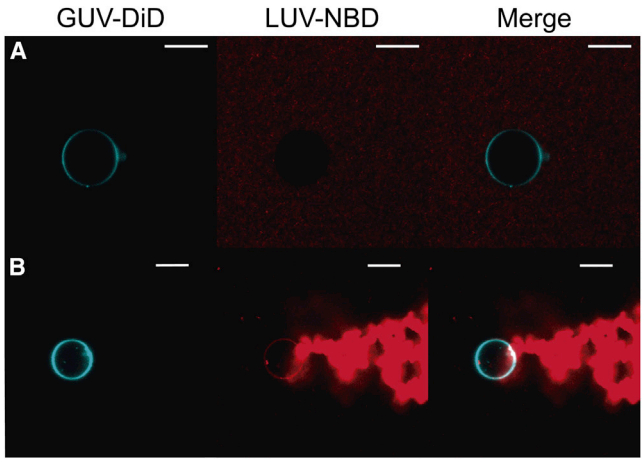

FIGURE 5 Inner lipid mixing observed by confocal microscopy of representative PC/PIP (9:1) GUVs labeled with DiD (*blue*) and LUVs labeled with NBD-PE in the inner leaflet only (*red*). (*A*) Control images obtained when H1 was not present; the dye spectra do not overlap. (*B*) GUVs and LUVs after unlabeled H1 addition; dye overlapping is observed on the GUV membranes. Scale bars: 10 μm.

Release of vesicle aqueous contents and its mechanism

The possibility of histone-induced permeabilization of lipid bilayers was tested as described in Materials and Methods. When the permeability barriers of LUVs containing entrapped water-soluble fluorescent probes lose their integrity, the probes diffuse rapidly to the outer aqueous medium, and this often leads to fluorescence changes that can be readily detected. In our case, the LUVs were loaded with the fluorescence emitter/fluorescence quencher complex ANTS/DPX. Upon release from the LUVs, the complex dissociated and ANTS fluorescence increased. Such an increase was clearly observed when histones were added to egg PC LUVs containing 10% of PI or PIP (Fig. 6 *A*), although the extent of release from the PIP vesicles was greater (Fig. 1 *B*). Different histones gave rise to different extents of leakage and leakage rates (Fig. 6 *C*) with both lipid compositions. H1-induced release of contents exhibited a considerably higher rate than any of the other three histone preparations, which could not be reliably measured.

Due to the fast H1-induced release of contents, the initial stages of the leakage process were undetectable by standard time-course recording methods (Fig. 6 *A*), so we used fast kinetics methods to visualize them (Fig. 7). Stopped-flow measurements revealed a considerably higher initial rate of H1-induced leakage when the bilayers contained PIP ($12.3 \pm 4.4\ s^{-1}$ (R^2 $0.998 \pm 1.5\ 10^{-3}$)) than when they contained PI ($0.21 \pm 0.01\ s^{-1}$ (R^2 $0.999 \pm 3.7\ 10^{-4}$)).

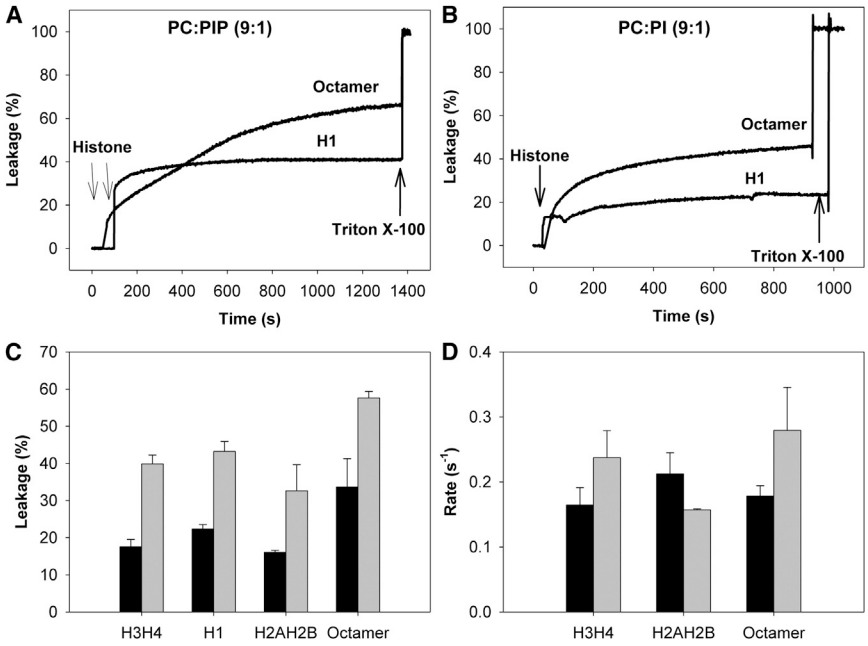

FIGURE 6 Histone-induced release of vesicular aqueous contents. Vesicle composition is indicated on top of the figure. (*A* and *B*) Time courses of vesicle leakage induced by H1 or octamer histones. Arrows indicate the histone or detergent addition. (*C*) Extent of leakage produced by different histones under apparent equilibrium (~20 min). (*D*) Initial rates of leakage produced by the different histone preparations. Black bars correspond to PIP-containing LUVs and gray bars correspond to PI-containing LUVs. Average values + mean ± SE ($n = 3$).

To elucidate the mechanism behind this, we measured calcein lifetimes with respect to graded or all-or-none leakage (see Materials and Methods). We observed different leakage mechanisms depending on the lipid composition (PI or PIP; Fig. 8). In vesicles with 10% PI, there was no change in calcein lifetime when either H1 or the octamer was added to liposomes at increasing concentrations. Therefore, we concluded that the all-or-none leakage mechanism was operating (Fig. 8 *A*). However, in PIP-containing vesicles, the lifetime of entrapped calcein increased with histone concentration, revealing a graded leakage mechanism (Fig. 8 *B*).

DISCUSSION

The above results describe a model system of histone-induced fusion of phospholipid vesicles containing PIP.

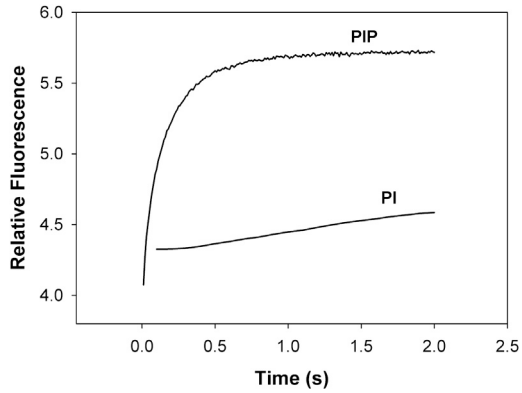

FIGURE 7 Early stages of H1-induced efflux of vesicular contents from LUVs containing 10 mol % of either PI or PIP. Stopped-flow assay.

Specifically, we found that vesicles containing PIP, but not those containing PI, can undergo fusion induced by histones. Moreover, in both PI- and PIP-containing vesicles, histones caused the permeabilization and release of vesicular aqueous contents. These events may have important physiological consequences. Below, we discuss the experimental data and their biological implications separately.

Vesicle-vesicle fusion

Our knowledge about biological membrane fusion, like so many other events in cell membrane physiology, has benefited from studies in model systems, including planar bilayers and liposomes (30–33). Early studies showed the importance of the vesicle lipid composition, including the net electrical charge (34–37). The use of fluorescent probes, pioneered by Wilschut and Papahadjopoulos (38), allowed investigators to distinguish among vesicle aggregation, intervesicular mixing, and intervesicular aqueous contents mixing (28), all of which must occur quasi-simultaneously for a phenomenon to be qualified as fusion. To our knowledge, studies in our laboratory were the first to describe model membrane fusion promoted by the catalytic activity of an enzyme, phospholipase C from *Bacillus cereus* (39). Later studies reported fusion induced by other phospholipases C and sphingomyelinases (16,26,40), and described intervesicular mixing of inner monolayer lipids as a novel marker for fusion (41). Montes et al. (16) described the time-resolved process of aggregation, total lipid mixing, inner monolayer lipid mixing, and aqueous contents mixing, which started with increasing lag times after enzyme addition.

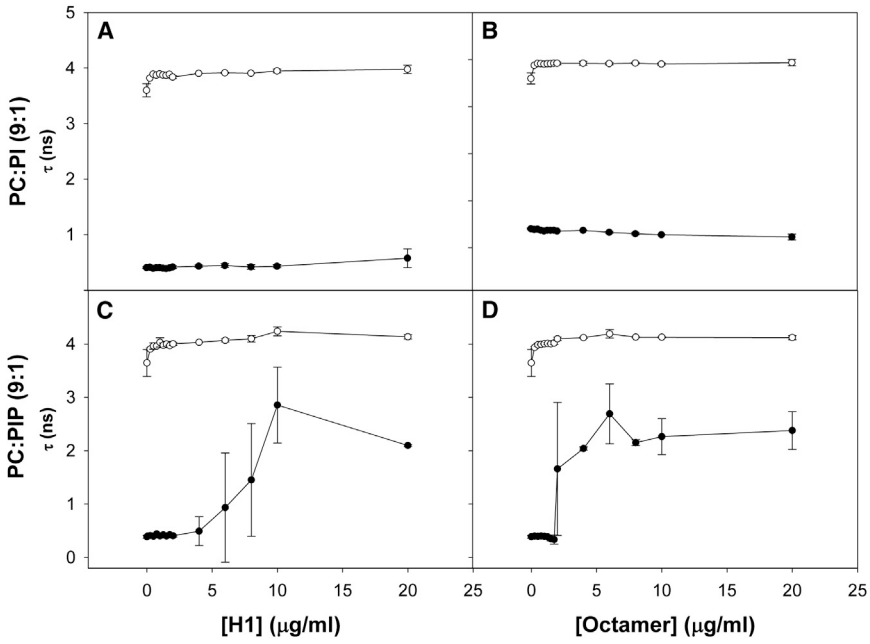

FIGURE 8 Mechanism of histone-induced vesicle leakage, deduced from fluorescence lifetime data. (*A–D*) LUVs (30 μM) were incubated for 1 h with H1 (*A* and *C*) or the histone octamer (*B* and *D*). The data correspond to the lifetimes of free calcein ($\approx$4 ns) (○) and entrapped calcein ($\approx$0.4 ns) (●). (*A* and *B*) PI-containing vesicles. (*C* and *D*) PIP-containing vesicles.

Liposome fusion induced by stoichiometric (as opposed to catalytic) amounts of protein has been described in the past (42,43). However, the physiological meaning of such fusion was not apparent. The above results (Figs. 1, 2, 3, 4, and 5) demonstrate that histones cause effects that in combination are diagnostic for membrane fusion. In our previous study (13), we showed that PIP could compete with DNA for histones. Together, our previous and current data suggest a complex multiple equilibrium in which free and bound DNA, free and bound histones (specifically H1) (44) and membranes, and nonfused and fused vesicles may coexist in the close vicinity of the nucleoplasmic reticulum.

The interaction of histones with vesicles containing either PI or PIP leads to the partial release of vesicular aqueous contents (Figs. 6, 7, and 8). This is a process that would interfere with the intervesicular mixing of aqueous contents, which is often used in vesicle fusion studies (28), but does not modify the more specific detection of inner monolayer lipid mixing (Figs. 1, 2, and 5) that we used in our experiments. The observation of leakage is interesting because it reveals a strong membrane-histone interaction. Membrane permeabilization, or leakage, is a process that is independent of membrane fusion, since fusion has been observed in both the absence (16,39) and presence (41,45) of leakage. In our case, it is interesting that PI- and PIP-containing vesicles were permeabilized by histones via two different mechanisms (Fig. 8). In our previous studies of histone-induced vesicle aggregation (13), the difference between the two kinds of vesicles was merely qualitative, with aggregation being more extensive in the presence of PIP. However, the different leakage mechanisms illustrate a qualitative difference in this case, which may be related to the fact that only in the presence of PIP do histones induce lipid mixing and fusion (Figs. 1, 2, and 3). This observation deserves further detailed studies.

Biological significance

The results presented here do not prove that histones promote fusion events at the nuclear membrane, but they do show that this is a possible outcome, especially considering that H1 is a dynamic histone and its interactions with the nucleosome are of a temporary nature (44). Furthermore, a number of previous findings provide additional support for our hypothesis that what we observe in the model system reflects the dynamics of formation and deformation of the NE during open mitosis. These findings include 1) an unexpectedly high concentration of polyphosphoinositides in certain fractions/domains of the NE (46); 2) evidence of multiple membrane fusion events during NE reformation (7), in which histones could play a helping or potentiating role in phospholipase C-induced fusion; 3) acute depletion of PI(4,5)P_2 results in incomplete NE reformation (47); and 4) morphological observations (old and new (4,47–49)) that present the nuclear membrane as consisting of a convoluted lamellar and tubular system penetrating the nuclear core. Finally, the relevance of the nucleoplasmic reticulum in a series of pathological conditions (e.g., cell malignancy, laminopathies, and viral access to the nucleoplasm (50,51)) provides a further degree of biological significance to our studies.

SUPPORTING MATERIAL

One figure is available at http://www.biophysj.org/biophysj/supplemental/S0006-3495(14)04763-8.

AUTHOR CONTRIBUTIONS

M.G.L. performed research, analyzed data, and wrote the article. J.S. and D.G. performed research and contributed analytical tools. M.V. contributed analytical tools, analyzed data, and wrote the article. M.M. contributed analytical tools and analyzed data. F.M.G. and A.A. designed research, analyzed data, and wrote the article.

ACKNOWLEDGMENTS

This work was supported in part by grants from the Spanish Ministry of Economy (BFU 2011-28566 to A.A., BFU 2012-36241 to F.M.G., and BIO 2013-42978-P to M.M.) and the Basque Government (IT 838-13 and IT 849-13). M.G.L. was a predoctoral student supported by the Basque Government.

REFERENCES

1. Mima, J., C. M. Hickey, …, W. Wickner. 2008. Reconstituted membrane fusion requires regulatory lipids, SNAREs and synergistic SNARE chaperones. *EMBO J.* 27:2031–2042.
2. Lynch, K. L., R. R. Gerona, …, T. F. Martin. 2008. Synaptotagmin-1 utilizes membrane bending and SNARE binding to drive fusion pore expansion. *Mol. Biol. Cell.* 19:5093–5103.
3. James, D. J., C. Khodthong, …, T. F. Martin. 2008. Phosphatidylinositol 4,5-bisphosphate regulates SNARE-dependent membrane fusion. *J. Cell Biol.* 182:355–366.
4. Irvine, R. F. 2006. Nuclear inositide signalling — expansion, structures and clarification. *Biochim. Biophys. Acta.* 1761:505–508.
5. Fili, N., V. Calleja, …, B. Larijani. 2006. Compartmental signal modulation: endosomal phosphatidylinositol 3-phosphate controls endosome morphology and selective cargo sorting. *Proc. Natl. Acad. Sci. USA.* 103:15473–15478.
6. Dumas, F., R. D. Byrne, …, B. Larijani. 2010. Spatial regulation of membrane fusion controlled by modification of phosphoinositides. *PLoS ONE.* 5:e12208.
7. Byrne, R. D., M. Garnier-Lhomme, …, B. Larijani. 2007. PLCγ is enriched on poly-phosphoinositide-rich vesicles to control nuclear envelope assembly. *Cell. Signal.* 19:913–922.
8. Malhas, A., C. Goulbourne, and D. J. Vaux. 2011. The nucleoplasmic reticulum: form and function. *Trends Cell Biol.* 21:362–373.
9. Goulbourne, C. N., A. N. Malhas, and D. J. Vaux. 2011. The induction of a nucleoplasmic reticulum by prelamin A accumulation requires CTP:phosphocholine cytidylyltransferase-α. *J. Cell Sci.* 124:4253–4266.
10. Pereira, L. F., F. M. Marco, …, J. L. Subiza. 1994. Histones interact with anionic phospholipids with high avidity; its relevance for the binding of histone-antihistone immune complexes. *Clin. Exp. Immunol.* 97:175–180.
11. Kõiv, A., J. Palvimo, and P. K. Kinnunen. 1995. Evidence for ternary complex formation by histone H1, DNA, and liposomes. *Biochemistry.* 34:8018–8027.
12. Zhao, H., S. Bose, …, P. K. Kinnunen. 2004. Interactions of histone H1 with phospholipids and comparison of its binding to giant liposomes and human leukemic T cells. *Biochemistry.* 43:10192–10202.
13. Lete, M. G., J. Sot, …, A. Alonso. 2014. Histones and DNA compete for binding polyphosphoinositides in bilayers. *Biophys. J.* 106:1092–1100.
14. Cocco, L., R. S. Gilmour, …, R. F. Irvine. 1987. Synthesis of polyphosphoinositides in nuclei of Friend cells. Evidence for polyphosphoinositide metabolism inside the nucleus which changes with cell differentiation. *Biochem. J.* 248:765–770.
15. Goñi, F. M., and A. Alonso. 2000. Membrane fusion induced by phospholipase C and sphingomyelinases. *Biosci. Rep.* 20:443–463.
16. Montes, L. R., M. Ibarguren, …, A. Alonso. 2007. Leakage-free membrane fusion induced by the hydrolytic activity of PlcHR(2), a novel phospholipase C/sphingomyelinase from Pseudomonas aeruginosa. *Biochim. Biophys. Acta.* 1768:2365–2372.
17. Terasaki, M., T. Shemesh, …, M. M. Kozlov. 2013. Stacked endoplasmic reticulum sheets are connected by helicoidal membrane motifs. *Cell.* 154:285–296.
18. Rothman, J. E., and G. Warren. 1994. Implications of the SNARE hypothesis for intracellular membrane topology and dynamics. *Curr. Biol.* 4:220–233.
19. Chernomordik, L. V., and M. M. Kozlov. 2008. Mechanics of membrane fusion. *Nat. Struct. Mol. Biol.* 15:675–683.
20. Wang, X., S. C. Moore, …, J. Ausió. 2000. Acetylation increases the α-helical content of the histone tails of the nucleosome. *J. Biol. Chem.* 275:35013–35020.
21. Mayer, L. D., M. J. Hope, and P. R. Cullis. 1986. Vesicles of variable sizes produced by a rapid extrusion procedure. *Biochim. Biophys. Acta.* 858:161–168.
22. Böttcher, C. J. F., C. M. van Gent, and C. Fries. 1961. A rapid and sensitive sub-micro phosphorus determination. *Anal. Chim. Acta.* 24:203–204.
23. Struck, D. K., D. Hoekstra, and R. E. Pagano. 1981. Use of resonance energy transfer to monitor membrane fusion. *Biochemistry.* 20:4093–4099.
24. Chernomordik, L., A. Chanturiya, …, J. Zimmerberg. 1995. The hemifusion intermediate and its conversion to complete fusion: regulation by membrane composition. *Biophys. J.* 69:922–929.
25. Viguera, A. R., M. Mencía, and F. M. Goñi. 1993. Time-resolved and equilibrium measurements of the effects of poly(ethylene glycol) on small unilamellar phospholipid vesicles. *Biochemistry.* 32:3708–3713.
26. Montes, L. R., F. M. Goñi, …, A. Alonso. 2004. Membrane fusion induced by the catalytic activity of a phospholipase C/sphingomyelinase from Listeria monocytogenes. *Biochemistry.* 43:3688–3695.
27. Angelova, M. I., and I. Tsoneva. 1999. Interactions of DNA with giant liposomes. *Chem. Phys. Lipids.* 101:123–137.
28. Ellens, H., J. Bentz, and F. C. Szoka. 1985. H^+- and Ca^{2+}-induced fusion and destabilization of liposomes. *Biochemistry.* 24:3099–3106.
29. Patel, H. T., and C. Heerklotz. 2009. Characterizing vesicle leakage by fluorescence lifetime measurements. *Soft Matter.* 5:2849–2851.
30. Cohen, F. S., M. H. Akabas, …, A. Finkelstein. 1984. Parameters affecting the fusion of unilamellar phospholipid vesicles with planar bilayer membranes. *J. Cell Biol.* 98:1054–1062.
31. Karatekin, E., and J. E. Rothman. 2012. Fusion of single proteoliposomes with planar, cushioned bilayers in microfluidic flow cells. *Nat. Protoc.* 7:903–920.
32. Bental, M., P. I. Lelkes, …, J. Wilschut. 1984. Ca^{2+}-independent, protein-mediated fusion of chromaffin granule ghosts with liposomes. *Biochim. Biophys. Acta.* 774:296–300.
33. Düzgüneş, N., H. Faneca, and M. C. Lima. 2010. Methods to monitor liposome fusion, permeability, and interaction with cells. *Methods Mol. Biol.* 606:209–232.
34. Saez, R., F. M. Goñi, and A. Alonso. 1985. The effect of bilayer order and fluidity on detergent-induced liposome fusion. *FEBS Lett.* 179:311–315.
35. Schneider, H., J. J. Lemasters, …, C. R. Hackenbrock. 1980. Liposome-mitochondrial inner membrane fusion. Lateral diffusion of integral electron transfer components. *J. Biol. Chem.* 255:3748–3756.
36. Wilschut, J., N. Düzgüneş, …, D. Papahadjopoulos. 1980. Studies on the mechanism of membrane fusion: kinetics of calcium ion induced

fusion of phosphatidylserine vesicles followed by a new assay for mixing of aqueous vesicle contents. *Biochemistry.* 19:6011–6021.

37. Papahadjopoulos, D., S. Hui, …, G. Poste. 1976. Studies on membrane fusion. I. Interactions of pure phospholipid membranes and the effect of myristic acid, lysolecithin, proteins and dimethylsulfoxide. *Biochim. Biophys. Acta.* 448:254–264.
38. Wilschut, J., and D. Papahadjopoulos. 1979. Ca^{2+}-induced fusion of phospholipid vesicles monitored by mixing of aqueous contents. *Nature.* 281:690–692.
39. Nieva, J. L., F. M. Goñi, and A. Alonso. 1989. Liposome fusion catalytically induced by phospholipase C. *Biochemistry.* 28:7364–7367.
40. Ruiz-Argüello, M. B., F. M. Goñi, and A. Alonso. 1998. Vesicle membrane fusion induced by the concerted activities of sphingomyelinase and phospholipase C. *J. Biol. Chem.* 273:22977–22982.
41. Villar, A. V., A. Alonso, and F. M. Goñi. 2000. Leaky vesicle fusion induced by phosphatidylinositol-specific phospholipase C: observation of mixing of vesicular inner monolayers. *Biochemistry.* 39:14012–14018.
42. Morero, R. D., A. L. Viñals, …, R. N. Farías. 1985. Fusion of phospholipid vesicles induced by muscle glyceraldehyde-3-phosphate dehydrogenase in the absence of calcium. *Biochemistry.* 24:1904–1909.
43. Caaveiro, J. M., A. Molina, P. Rodriguez-Palenzuela, F. M. Goni, and J. M. Gonzalez-Manas. 1998. Interaction of wheat α-thionin with large unilamellar vesicles. *Protein Sci.* 7:2567–2577.
44. Bustin, M., F. Catez, and J. H. Lim. 2005. The dynamics of histone H1 function in chromatin. *Mol. Cell.* 17:617–620.
45. Nieva, J. L., S. Nir, …, J. Wilschut. 1994. Interaction of the HIV-1 fusion peptide with phospholipid vesicles: different structural requirements for fusion and leakage. *Biochemistry.* 33:3201–3209.
46. Garnier-Lhomme, M., R. D. Byrne, …, B. Larijani. 2009. Nuclear envelope remnants: fluid membranes enriched in sterols and polyphosphoinositides. *PLoS ONE.* 4:e4255.
47. Domart, M. C., T. M. Hobday, …, B. Larijani. 2012. Acute manipulation of diacylglycerol reveals roles in nuclear envelope assembly & endoplasmic reticulum morphology. *PLoS ONE.* 7:e51150.
48. Fricker, M., M. Hollinshead, …, D. Vaux. 1997. The convoluted nucleus. *Trends Cell Biol.* 7:181.
49. Echevarría, W., M. F. Leite, …, M. H. Nathanson. 2003. Regulation of calcium signals in the nucleus by a nucleoplasmic reticulum. *Nat. Cell Biol.* 5:440–446.
50. Malhas, A. N., and D. J. Vaux. 2014. Nuclear envelope invaginations and cancer. *Adv. Exp. Med. Biol.* 773:523–535.
51. De Vos, W. H., F. Houben, …, J. L. Broers. 2011. Repetitive disruptions of the nuclear envelope invoke temporary loss of cellular compartmentalization in laminopathies. *Hum. Mol. Genet.* 20:4175–4186.